Mutational landscape, clonal evolution patterns, and role of RAS mutations in relapsed acute lymphoblastic leukemia

Koichi Oshima[a,1], Hossein Khiabanian[b,c,d,1], Ana C. da Silva-Almeida[a], Gannie Tzoneva[a], Francesco Abate[b,c], Alberto Ambesi-Impiombato[a], Marta Sanchez-Martin[a], Zachary Carpenter[b,c], Alex Penson[b,c], Arianne Perez-Garcia[a], Cornelia Eckert[e,f], Concepción Nicolas[g], Milagros Balbin[h], Maria Luisa Sulis[i], Motohiro Kato[j], Katsuyoshi Koh[j], Maddalena Paganin[k], Giuseppe Basso[k], Julie M. Gastier-Foster[l,m,n,o], Meenakshi Devidas[p], Mignon L. Loh[q,r], Renate Kirschner-Schwabe[e,f], Teresa Palomero[a,s,2], Raul Rabadan[b,c,2], and Adolfo A. Ferrando[a,i,s,2]

[a]Institute for Cancer Genetics, Columbia University, New York, NY 10032; [b]Department of Systems Biology, Columbia University, New York, NY 10032; [c]Department of Biomedical Informatics, Columbia University, New York, NY 10032; [d]Rutgers Cancer Institute, Rutgers University, New Brunswick, NJ 08903; [e]Department of Pediatric Oncology/Hematology, Charité-Universitätsmedizin Berlin, 13353 Berlin, Germany; [f]German Cancer Consortium, German Cancer Research Center, 69120 Heidelberg, Germany; [g]Hematology Service, Hospital Central de Asturias, 33011 Oviedo, Spain; [h]Molecular Oncology Laboratory, Instituto Universitario de Oncologia del Principado de Asturias, Hospital Universitario Central de Asturias, 33011 Oviedo, Spain; [i]Department of Pediatrics, Columbia University Medical Center, New York, NY 10032; [j]Department of Hematology-Oncology, Saitama Children's Medical Center, Saitama 339-8551, Japan; [k]Onco-Hematology Division, Department, Salute della Donna e del Bambino (SDB), University of Padua, 35128 Padua, Italy; [l]Department of Pathology and Laboratory Medicine, Nationwide Children's Hospital, Columbus, OH 43205; [m]Department of Pathology, Ohio State University School of Medicine, Columbus, OH 43210; [n]Department of Pediatrics, Ohio State University School of Medicine, Columbus, OH 43210; [o]Children's Oncology Group, Arcadia, CA 91006; [p]Department of Biostatistics, University of Florida, Gainesville, FL 32611; [q]Department of Pediatrics, University of California, San Francisco, CA 94143; [r]Helen Diller Family Comprehensive Cancer Center, San Francisco, CA 94115; and [s]Department of Pathology, Columbia University Medical Center, New York, NY 10032

Edited by Louis M. Staudt, National Cancer Institute, NIH, Bethesda, MD, and approved August 9, 2016 (received for review May 25, 2016)

Although multiagent combination chemotherapy is curative in a significant fraction of childhood acute lymphoblastic leukemia (ALL) patients, 20% of cases relapse and most die because of chemorefractory disease. Here we used whole-exome and whole-genome sequencing to analyze the mutational landscape at relapse in pediatric ALL cases. These analyses identified numerous relapse-associated mutated genes intertwined in chemotherapy resistance-related protein complexes. In this context, RAS-MAPK pathway-activating mutations in the neuroblastoma RAS viral oncogene homolog (*NRAS*), kirsten rat sarcoma viral oncogene homolog (*KRAS*), and protein tyrosine phosphatase, nonreceptor type 11 (*PTPN11*) genes were present in 24 of 55 (44%) cases in our series. Interestingly, some leukemias showed retention or emergence of RAS mutant clones at relapse, whereas in others RAS mutant clones present at diagnosis were replaced by RAS wild-type populations, supporting a role for both positive and negative selection evolutionary pressures in clonal evolution of RAS-mutant leukemia. Consistently, functional dissection of mouse and human wild-type and mutant RAS isogenic leukemia cells demonstrated induction of methotrexate resistance but also improved the response to vincristine in mutant RAS-expressing lymphoblasts. These results highlight the central role of chemotherapy-driven selection as a central mechanism of leukemia clonal evolution in relapsed ALL, and demonstrate a previously unrecognized dual role of RAS mutations as drivers of both sensitivity and resistance to chemotherapy.

acute lymphoblastic leukemia | relapsed leukemia | chemotherapy resistance | genome sequencing

Acute lymphoblastic leukemia (ALL) is the most common malignancy in children (1–4). Current therapy of pediatric newly diagnosed ALL includes initial clearance of leukemic lymphoblasts with cytotoxic drugs and glucocorticoids followed by delivery of chemotherapy to the central nervous system and a prolonged lower intensity maintenance treatment phase aimed at securing long-term remission by reducing the rates of leukemia relapse (3). Altogether 95% of pediatric ALL patients achieve a complete hematologic remission during induction and 80% of them remain leukemia free (5). However, the prognosis of patients showing refractory disease or those whose leukemia relapses after an initial transient response remains disappointingly poor, with cure rates of less than 40% (6, 7). Several mechanisms have been implicated as drivers of leukemia relapse, including the presence of rare quiescent and intrinsically chemoresistant leukemia stem cells with increased self-renewal capacity (8), protection from chemotherapy by safe-haven microenvironment niches (9, 10), and selection of secondary genetic alterations promoting chemotherapy resistance in leukemic lymphoblasts (11–13). In this regard, early studies described the presence of tumor protein p53 (*TP53*) mutations in relapsed ALL, supporting a role for escape from genotoxic stress in leukemia progression (14). Similarly, loss of nuclear receptor subfamily 3 group C member 1 (*NR3C1*) encoding the glucocorticoid receptor has been associated with

Significance

Relapsed acute lymphoblastic leukemia (ALL) is associated with chemotherapy resistance and poor prognosis. This study analyzes the emergence of acquired mutations in relapsed ALL samples, identifying genes implicated in disease progression and defining the process of clonal evolution leading to relapse. These analyses revealed that ALL relapse emerges from subclonal populations sharing only part of the mutations present in the dominant leukemia population found at diagnosis. Moreover, we show mutations in genes implicated in chemotherapy resistance pathways at relapse. RAS mutations are highly prevalent in high-risk ALL, yet their capacity to confer resistance to methotrexate and sensitivity to vincristine, two core drugs used in the treatment of ALL, influences their positive or negative selection at relapse.

Author contributions: T.P., R.R., and A.A.F. designed research; K.O., A.C.d.S.-A., G.T., M.S.-M., A.P.-G., C.E., M.L.S., and T.P. performed research; C.N., M.B., M.L.S., M.K., K.K., M.P., G.B., J.M.G.-F., M.D., M.L.L., and R.K.-S. contributed new reagents/analytic tools; K.O., H.K., F.A., A.A.-I., Z.C., A.P., C.E., R.K.-S., R.R., and A.A.F. analyzed data; and K.O., H.K., T.P., and A.A.F. wrote the paper.

The authors declare no conflict of interest.

This article is a PNAS Direct Submission.

Data deposition: The sequences reported in this paper has been deposited in the dbGaP database (accession no. phs001072.v1.p1).

See Commentary on page 11071.

[1]K.O. and H.K. contributed equally to this work.

[2]To whom correspondence may be addressed. Email: af2196@columbia.edu, tp2151@columbia.edu, or rr2579@cumc.columbia.edu.

This article contains supporting information online at www.pnas.org/lookup/suppl/doi:10.1073/pnas.1608420113/-/DCSupplemental.

relapse in *ETV6-RUNX1* rearranged leukemias (15). In addition, mutations disrupting the genes encoding for the CREB binding protein (*CREBBP*), a histone acetyl transferase implicated in glucocorticoid response (16), and a number of other epigenetic factors (17) have been associated with relapse. Finally, genomic profiling of diagnostic and relapsed leukemias has identified relapse-associated mutations in the 5′-nucleotidase, cytosolic II (*NT5C2*) gene as drivers of resistance to thiopurine chemotherapy in about 20% of T-ALL and 5% of B-precursor ALL cases at relapse (11, 12, 18). However, the genomic landscape of relapse ALL remains largely unexplored, and the mechanisms mediating escape from therapy, disease progression, and leukemia relapse remain incompletely understood.

Results

To explore the landscape of genetic alterations involved in relapsed ALL, we performed whole-exome sequence analysis of matched diagnosis, germ line (remission), and relapse DNA samples in a panel of 55 pediatric ALL patients including 33 T-cell ALLs and 22 B-cell precursor ALLs (Datasets S1 and S2). Somatic mutation variant calling using the SAVI algorithm (19) identified an average of nine mutations present in diagnostic samples and 17 mutations in relapsed leukemia DNAs (*SI Appendix*, Figs. S1 and S2 and Datasets S3 and S4). Recurrently somatically mutated genes in our series included known oncogenes and tumor suppressors mutated in B-cell precursor ALL [*KRAS*, *NRAS*, Fms related tyrosine kinase 3 (*FLT3*), Janus kinase 2 (*JAK2*), Janus kinase 3 (*JAK3*), and *CREBBP*] (20) and T-cell ALL [Notch1 (*NOTCH1*), *FBXW7*, *PHF6*, *DNM2*, *WT1*, *JAK1*, *JAK3*, *BCL11B*, *TP53*, *CREBBP*, *RPL10*, *RUNX1*, and *CNOT3*] (16, 21–27). In addition, we also identified recurrently ALL mutated genes including *ZFHX3*, ubiquitin specific peptidase 9, X-linked (*USP9X*), calcium voltage-gated channel subunit alpha1 H (*CACNA1H*), *EPHA3*, *SHROOM3*, *USP7*, *RPGR*, 5-hydroxytryptamine receptor 3A (*HTR3A*), mediator complex subunit 12 (*MED12*), teneurin transmembrane protein 3 (*TENM3*), and *IL17RA* (Fig. 1, *SI Appendix*, Fig. S3, and Datasets S3 and S4). Copy number analyses identified an average of 10.4 somatic copy number variants (CNVs) per sample (8.7 in T-cell ALL and 13.1 in B-cell precursor ALL) for a total of 501 alterations in our series. Of these, 248 CNVs were detected at diagnosis and 253 at the time of relapse, with 180 variants present in both diagnostic and relapsed samples (*SI Appendix*, Figs. S4 and S5 and Dataset S5).

Analysis of clonal evolution dynamics of relapsed ALL revealed a branched pattern of clonal evolution in 41 of 48 (85%) of the cases in which relapsed samples contained only some of the genetic lesions present in the major clone at diagnosis (Fig. 2 and *SI Appendix*, Fig. S6). In addition, five relapsed leukemia samples in this series (samples 5, 9, 14, 18, and 38) contained most but not all of the mutations present at diagnosis. Finally, in the remaining 2 of the 48 (4%) cases (samples 21 and 39), the relapsed clones contained all protein-coding genetic mutations present at diagnosis plus additional secondary relapse-specific lesions. For these and for an additional case with a pattern at the boundary between linear and branched evolution (sample 38), we performed whole-genome sequencing of matched diagnosis, germ line (remission), and relapse DNA samples (*SI Appendix*, Fig. S7 and Dataset S6). We identified 3,868 noncoding mutations including 394 located <5 Kb downstream, 1,762 intergenic, 1,621 intronic, 81 <5 Kb upstream, 7 UTR 3′, 2 UTR 5′, and 1 intragenic variants. Of these, 51 were diagnosis-specific, 1,892 were relapse-specific, and 1,925 were shared between both relapse and diagnosis. These analyses demonstrated clear branched evolution, with the emergence of relapse clones showing partial overlap with the mutations present at diagnosis and containing additional relapse-specific mutations in all three cases analyzed (*SI Appendix*, Fig. S7). These results support that linear evolution is rarely involved in tumor progression and that relapsed ALLs originate primarily by branched evolution as derivates of ancestral subclones related to but distinct from the main leukemic population present at diagnosis (*SI Appendix*, Fig. S8).

Several relapse ALL-associated mutant genes were functionally related to the mechanisms of action of chemotherapy. We identified the presence of heterozygous, relapse-specific mutations in the *NT5C2* gene, which encodes a cytosolic nucleotidase involved in the clearance of cytotoxic metabolites of 6-thioguanine and 6-mercaptopurine in 10 of 55 (18%) cases [1 of 22 (5%) in B-cell precursor ALL; 9 of 33 (27%) in T-cell ALL]. These included three previously characterized gain-of-function *NT5C2* alleles (NT5C2 R238W, NT5C2 K359Q, and NT5C2 R367Q) involved in thiopurine resistance (11, 12), two mutations at positions altered in previously reported *NT5C2* gain-of-function alleles [NT5C2 D407E and NT5C2 (S445F,R446Q)], and one *NT5C2*-activating mutation (NT5C2 R478S) (Fig. 1*B*, *SI Appendix*, Fig. S9, and Dataset S3). We also identified three T-cell ALLs with mutations in the *TP53* gene (3 of 33, 9%), one of which was specifically selected at the time of relapse (Fig. 1 *A* and *B*, *SI Appendix*, Fig. S3, and Dataset S3), and two relapsed-specific mutations in the glucocorticoid receptor gene (*NR3C1*) (Fig. 1 *A* and *B*, *SI Appendix*, Fig. S3, and Dataset S3). Ultra-deep sequencing analysis of *NT5C2* ($n = 7$), *TP53* ($n = 2$), and *NR3C1* ($n = 2$) mutations in the corresponding diagnostic DNA samples failed to identify these resistance-driving mutations with 0.5% sensitivity, suggesting that they were present in small subclones or were acquired during disease progression. In addition, we identified truncating mutations and single amino acid substitutions disrupting the histone acetyl-transferase domain of *CREBBP* in four cases [4 of 55 (7%); 2 of 22 (9%) B-cell precursor ALLs; 2 of 33 (6%) T-cell ALLs], including three patients with mutations positively selected at the time of relapse (Fig. 1 *A* and *D*, *SI Appendix*, Fig. S3, and Dataset S3). Further analysis of relapse-associated epigenetic factor mutations in our series revealed 3 of 55 (5%) mutations in the lysine methyltransferase 2D (*KMT2D*) gene, also known as myeloid/lymphoid or mixed-lineage leukemia 2 (*MLL2*), two of which were selected at relapse (Fig. 1 *A* and *D*, *SI Appendix*, Fig. S3, and Dataset S3). However, 23 of 27 (85%) of all recurrently mutated genes in this series whose mutations were preferentially selected or retained at the time of relapse (mutation never lost in the relapse clone) were not previously implicated in relapse ALL (*HTR3A*, *MED12*, *USP9X*, *CACNA1H*, *TENM3*, *AACS*, *SAMD4A*, *ANO5*, *PAPPA*, *NAALADL2*, *HIST3H2A*, *FZD7*, *TBX15*, *NEB*, *GREB1L*, *PLXNA4*, *SGK223*, *TSC1*, *PTPRG*, *FGF10*, *SYCP2*, *TRPM3*, and *EYS*) (Fig. 1 *A* and *C–E*, *SI Appendix*, Fig. S3, and Dataset S4). Orthogonal mutation analysis of 18 genes harboring recurrent mutations positively selected during disease progression in a series of 49 paired diagnosis and relapse B-cell precursor ALL cases analyzed by RNA-seq (Dataset S7) and in an extended series of 230 relapsed B-cell precursor ALLs evaluated by targeted deep sequencing (Dataset S8) confirmed and extended these results, revealing additional mutations in *NT5C2* (13 of 279, 4.6%), *NR3C1* (7 of 279, 2.5%), *CREBBP* (29 of 279, 10%), *KMT2D* (11 of 279, 4%), *JAK2* (17 of 279, 6%), *JAK3* (18 of 279, 6.5%), and *TP53* (18 of 279, 6.5%) (*SI Appendix*, Fig. S10). In all, 160 of 279 (57%) cases in these validation series showed at least one driver relapse-associated mutation. In addition, analysis of experimentally established protein–protein interactions across the products of 153 genes harboring at least one mutation gained at relapse in our series revealed a network structure in which most interactions converged on a limited number of highly connected proteins (*SI Appendix*, Fig. S11). Notably, the highest connected nodes in this circuitry encompassed the products of key genes whose mutations can drive chemotherapy resistance (*TP53*, *CREBBP*, and *NR3C1*) (*SI Appendix*, Fig. S11).

An additional notable finding in our relapsed ALL exome mutation analysis was the presence of highly prevalent mutations activating the RAS-MAPK signaling pathway (Fig. 1*C* and *SI Appendix*, Fig. S3). These included activating mutations in *KRAS* in 11 of 55 (20%) cases (7 of 22, 32% B-precursor ALL; 4 of 33, 12% T-ALL), gain-of-function mutations in *NRAS* in 13 of 55 (24%)

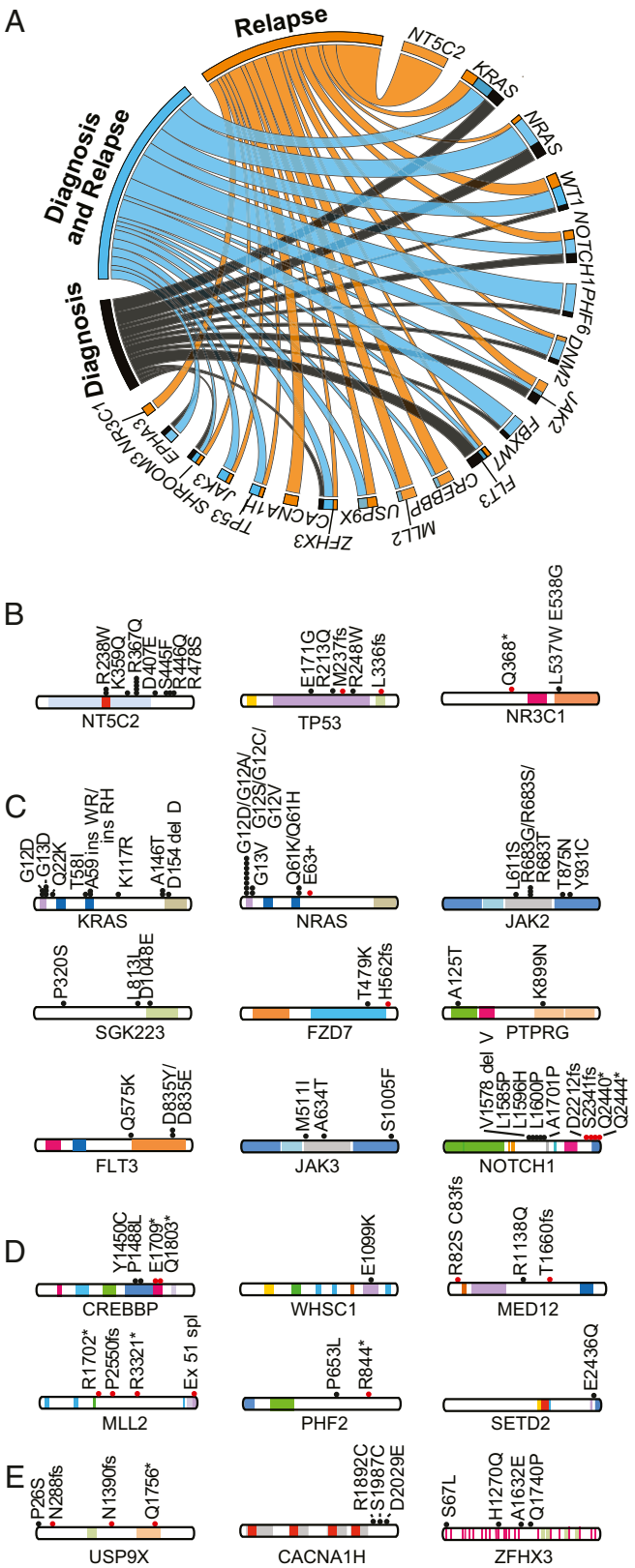

Fig. 1. Somatic mutations in relapsed ALL. (*A*) Circus plot representation of the distribution of diagnostic, relapse, and common diagnosis and relapse mutations involving selected recurrently mutated genes. (*B*–*E*) Schematics of the protein structures showing mutations recurrently identified in diagnostic and relapse ALL samples. Proteins involved in chemotherapy resistance (*B*), signaling (*C*), epigenetic regulation (*D*), and other recurrently mutated factors (*E*) are represented. Black circles indicate amino acid substitutions; red circles indicate truncating mutations.

cases (4 of 22, 18% B-precursor ALL; 9 of 33, 27% T-ALL), and one activating mutation in the *PTPN11* (PTPN11 G503R) phosphatase gene previously reported in Noonan syndrome (28, 29) (Fig. 1*C*, *SI Appendix*, Fig. S3, and Dataset S3). Similar results were observed in our validation cohort of paired diagnosis and relapse samples analyzed by RNA-seq [*KRAS* mutations, 9 of 49 (18%); *NRAS* mutations, 12 of 49 (20%)] and in our panel of relapsed samples analyzed by targeted deep sequencing [*KRAS* mutations, 35 of 230 (15%); *NRAS* mutations, 32 of 230 (15%)] for an overall prevalence of 113 of 334 (34%) RAS-MAPK–activating mutations in high-risk ALL. The high prevalence of RAS mutations in our relapsed leukemia series is consistent with previous reports (18, 30, 31) and differs from the results obtained from the analysis of unselected pediatric ALLs, which showed a markedly lower frequency of activating mutations in *NRAS* (5 of 41, 12%) and *KRAS* (0 of 41, 0%) (Fisher's exact test $P < 0.005$), suggesting that aberrant MAPK signaling could be a prominent driver oncogenic mechanism in high-risk ALL. However, we noted that although most cases with *NRAS* and *KRAS* mutations present at diagnosis were recovered at relapse (12 of 24, 50%) and others showed emergence of a different RAS mutant allele (1 of 24, 4%) or of new RAS mutant clones at relapse (6 of 24, 25%), some patients with *NRAS* and *KRAS* mutations at diagnosis relapsed at the expense of RAS wild-type clones (5 of 24, 21%).

To evaluate the specific role of RAS-MAPK–activating mutations in chemotherapy resistance, we generated isogenic leukemias via retroviral transduction and bone marrow transplantation of hematopoietic progenitors from Lox–stop–lox (LSL)-*Kras*^{G12D} mice (32) infected with retroviruses expressing an oncogenic form of NOTCH1 (ΔE-NOTCH1) (*SI Appendix*, Fig. S12). In this model, introduction of Cre recombinase induces the expression of the mutant *Kras* G12D from the endogenous *Kras* locus with consequent activation-increased MAPK signaling (Fig. 3 *A* and *B* and *SI Appendix*, Fig. S13). Notably, drug response analyses in isogenic *Kras* wild-type and *Kras* G12D cells showed increased resistance to methotrexate ($P < 0.001$) upon oncogenic Kras activation (Fig. 3 *C*–*E* and *SI Appendix*, Fig. S14). Consistently, *Kras* G12D mutant cells were enriched over their *Kras* wild-type counterparts in mixed cultures under selection with methotrexate (*SI Appendix*, Fig. S15). Moreover, suppression of MAPK signaling with the U0126 and the PD0325901 MEK inhibitors (33) showed increased antileukemic activity in *Kras* G12D mutant cells and enhanced the cytotoxic activity of methotrexate (Fig. 3 *F* and *G* and *SI Appendix*, Figs. S16–S20). Furthermore, expression of activating mutant KRAS proteins in human CUTLL1 and JURKAT ALL cell lines induced resistance to methotrexate chemotherapy (Fig. 3 *H* and *I* and *SI Appendix*, Figs. S21 and S22). Notably, this methotrexate resistance phenotype correlated with the strength of MAPK activation as expression of a double KRAS G12D Q61R mutation induced higher levels of MAPK phosphorylation and more robust methotrexate resistance than expression of the single KRAS Q61R mutant allele (Fig. 3 *H* and *I*). There were no significant differences in the response to dexamethasone, daunorubicin, cytarabine, and mafosfamide between mutant *Kras* G12D and isogenic wild-type ALL cells (*SI Appendix*, Fig. S23). However, we observed a reproducible increased sensitivity to vincristine treatment in *Kras* G12D mutant cells with decreased viability (Fig. 4*A* and *SI Appendix*, Fig. S14), increased apoptosis (Fig. 4 *B* and *C*), and enhanced G2/M cell-cycle arrest (Fig. 4 *D* and *E* and *SI Appendix*, Fig. S24) compared with wild-type isogenic controls. Moreover, *Kras* wild-type cells were enriched over their isogenic *Kras* G12D mutant counterpart cells in mixed cultures under vincristine selection (*SI Appendix*, Fig. S25). Of note, Kras activation was associated with increased Polo-like

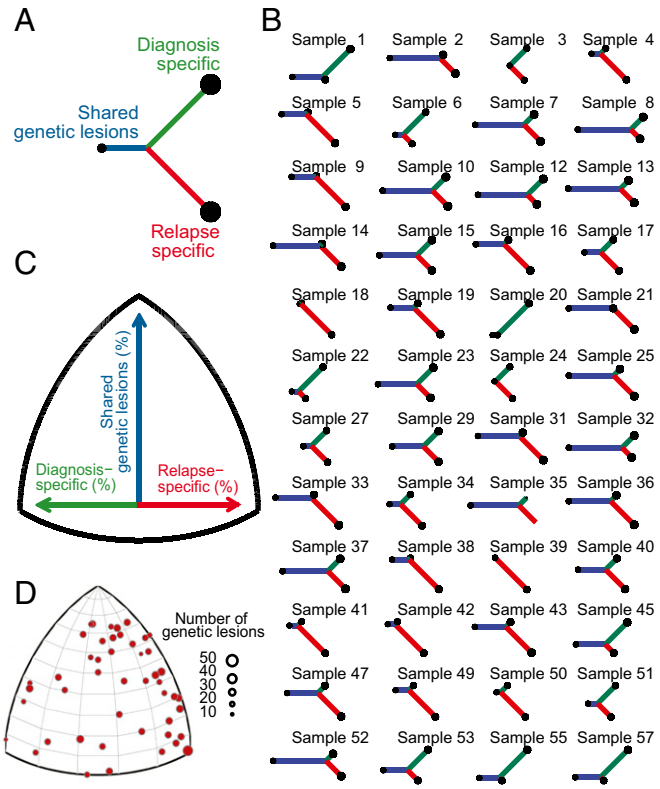

Fig. 2. Clonal evolution in relapsed ALL. (*A*) Graphical representation of the evolutionary history of ALL based on mutation and copy number alteration analysis. The sizes of the nodes and the lengths of the branches in the evolutionary tree graph indicate the percentage of shared, diagnosis-specific, and relapse-specific genetic alterations in each sample. (*B*) Evolutionary trees of 48 diagnostic remission and relapse paired samples evaluated by whole-exome sequencing. (*C*) Projection of the shared, diagnosis-specific, and relapse-specific genetic alterations (i.e., scaling by the total number of alterations) shows the evolutionary history of each leukemia as a single point. In this graph, the higher the percentage of relapse-specific mutations in a sample, the closer its corresponding point to the right edge of the triangle; the higher the percentage of diagnosis-specific mutations in a sample, the closer its corresponding point to the left edge of the triangle; and the higher the number of shared mutations in a sample, the closer its corresponding point to the top corner. (*D*) Projected evolutionary history of 48 analyzed ALLs, in which patients are represented by circles, scaled by their total number of mutations. When two trees have similar evolutionary histories, they will be projected closely, despite possible differences in their branch lengths and node sizes.

Kinase 1 activation loop phosphorylation (T210) (Fig. 4*F*), a post-translational modification implicated in the control of mitotic entry (34) and recovery after checkpoint-dependent G2 arrest (35, 36). Moreover RNA-seq analysis of isogenic *Kras* G12D and *Kras* wild-type cells showed down-regulation of mitotic signature genes upon activation of oncogenic Kras (Fig. 4*G*), further supporting a role of mutant Kras in mitotic deregulation. As before, expression of mutant *KRAS* in human ALL cell lines increased sensitivity to vincristine (Fig. 4*H* and *SI Appendix*, Fig. S26). Finally, gene expression analyses of human B-precursor ALLs with or without *KRAS* mutations revealed a significant enrichment of a gene signature associated with increased sensitivity to vincristine (37) in *KRAS* mutant samples (Fig. 4 *I* and *J*), an effect confirmed in analogous analyses using expression signatures associated with *KRAS* and *NRAS* mutant samples (*SI Appendix*, Fig. S27).

Discussion

Here we have dissected the mutational landscape of relapsed ALL, analyzed the pattern of clonal evolution associated with relapse in this disease, and explored the mechanisms underlying the mixed pattern of positive and negative selection of RAS mutations associated with leukemia progression. Consistent with previous genomic studies (26, 38), pediatric ALL leukemia samples in our series showed a low burden of exonic mutations and copy number alterations at diagnosis. Moreover, and with the exception of one T-ALL tumor, which showed a marked increase in mutation load at relapse, the mutation load of these leukemias was only modestly increased at relapse. Mechanistically, mutation pattern analyses support that ALL mutations originate by spontaneous deaminations during tumor initiation and that this mutation mechanism is also characteristic at the time of relapse (39). A corollary of these findings is that chemical mutagenesis, characteristically associated with increased frequency of transversions (40), does not seem to represent a major driver of tumor initiation or relapse-associated mutations in ALL. This is in contrast with findings in acute myeloid leukemia, where analysis of relapse genomes has evidenced an

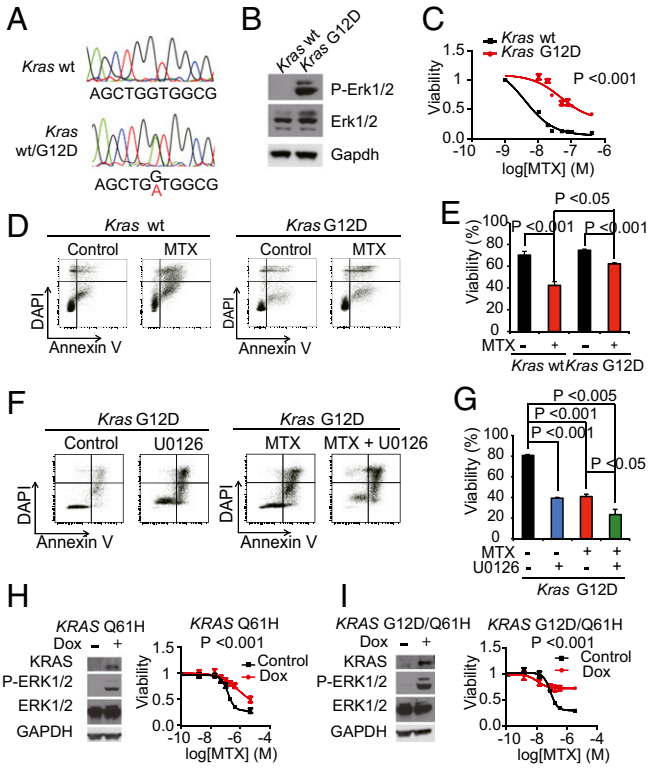

Fig. 3. Methotrexate resistance induced by *Kras* G12D expression in ALL. (*A*) Kras cDNA sequencing results from mouse *Kras* wild-type (*Kras* wt/LSL-*Kras* G12D genotype) and isogenic *Kras* G12D (*Kras* wt/*Kras* G12D genotype) ALL cells. (*B*) Western blot analysis of Erk activation in mouse *Kras* wild-type and isogenic *Kras* G12D ALL cells. (*C*) Cell viability assays in mouse *Kras* wild-type and isogenic *Kras* G12D-expressing ALL cells treated with methotrexate (MTX). (*D*) Representative dot plots of flow cytometry analysis of cell viability and apoptosis in mouse *Kras* wild-type and isogenic *Kras* G12D-expressing ALL cells treated with methotrexate (25 nM) for 48 h. (*E*) Quantitative analysis of cell viability in mouse *Kras* wild-type and isogenic *Kras* G12D-expressing ALL cells treated with methotrexate (25 nM) for 48 h. (*F*) Representative dot plots of flow cytometry analysis of cell viability and apoptosis in mouse *Kras* G12D-expressing ALL cells treated with methotrexate (30 nM) and U0126 (2 μM) for 48 h. (*G*) Quantitative analysis of cell viability of mouse *Kras* G12D-expressing ALL cells treated with methotrexate (30 nM) and U0126 (2 μM) for 48 h. (*H*) Western blot analysis of RAS expression and Erk activation and viability assays in CUTLL1 ALL cells treated with methotrexate in basal conditions (Vehicle) and upon doxycycline-induced (Dox 100 ng/mL) KRAS Q61H expression. (*I*) Western blot analysis of RAS expression and Erk activation and viability assays in CUTLL1 ALL cells treated with methotrexate in basal conditions (Vehicle) and upon doxycycline-induced (Dox 100 ng/mL) KRAS G12D/Q61H double-mutant expression. Quantitative data are shown as means ± SD.

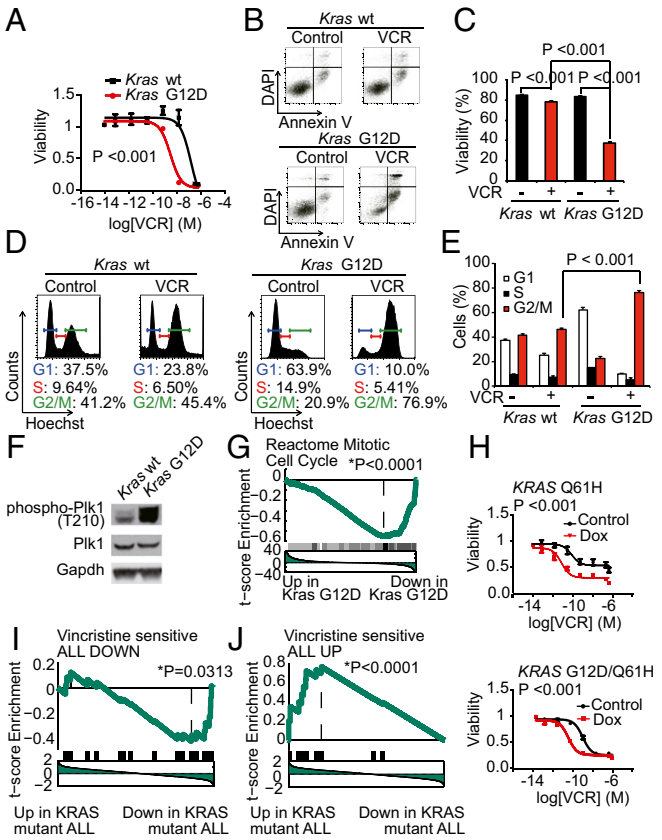

Fig. 4. Vincristine sensitivity induced by *Kras* G12D expression in ALL. (*A*) Cell viability assays in mouse *Kras* wild-type and isogenic *Kras* G12D-expressing ALL cells treated with vincristine (VCR). (*B*) Representative dot plots of flow cytometry analysis of cell viability and apoptosis in mouse *Kras* wild-type and isogenic *Kras* G12D-expressing ALL cells treated with vincristine (5 nM) for 24 h. (*C*) Quantitative analysis of cell viability in mouse *Kras* wild-type and isogenic *Kras* G12D-expressing ALL cells treated with vincristine (5 nM) for 24 h. (*D*) Representative histograms of cell-cycle distribution in mouse *Kras* wild-type and isogenic *Kras* G12D-expressing ALL cells treated with vincristine (5 nM) for 24 h. (*E*) Quantitative analysis of cell-cycle distribution in mouse *Kras* wild-type and isogenic *Kras* G12D-expressing ALL cells treated with vincristine (5 nM) for 24 h. (*F*) Western blot analysis of Polo-like kinase 1 (Plk1) phosphorylation (T210) in mouse *Kras* wild-type and isogenic *Kras* G12D ALL cells. (*G*) Gene set enrichment plots corresponding to gene set enrichment analysis analysis of mitotic cell-cycle genes in the transcriptional signature of mouse *Kras* wild-type versus isogenic *Kras* G12D ALL cells. (*H*) Viability assays in CUTLL1 ALL cells treated with vincristine in basal conditions (Vehicle) and upon doxycycline-induced (Dox 100 ng/mL) expression of KRAS Q61H or the double mutant KRAS G12D/Q61H. (*I*) Gene set enrichment plot corresponding to GSEA analysis of genes down-regulated in vincristine sensitivity in relapsed B-ALLs with or without mutations in *KRAS*. (*J*) Gene set enrichment plot corresponding to GSEA analysis of genes up-regulated in vincristine sensitivity in relapsed B-ALLs with or without mutations in *KRAS*. Quantitative data are shown as means ± SD.

increased frequency of transversions probably derived from the mutagenic effects of chemotherapy (41). In this context, the cell of origin of relapse ALL seems to be exposed to limiting amounts of genotoxic stress, perhaps reflecting increased detoxifying drug-export or drug-metabolizing mechanisms.

Original analysis of clonal evolution in relapsed ALL based on the study of copy number alteration described different patterns of linear and branched clonal evolution in the context of relapsed ALL (42). However, combined analysis of clonal evolution integrating copy number alterations and exonic mutations in our series revealed a marked dominance of branched evolution in which relapsed ALL populations originate from ancestral clones sharing some but not all mutations present in the diagnostic sample. This finding is in agreement with recent genomic studies in ALL (11, 18) and contrasts with clonal evolution studies in acute myeloid leukemia, which have documented a more heterogeneous pattern of clonal evolution with some relapses emerging as a result of branched evolution and others resulting from the linear acquisition of secondary mutations in the main diagnostic clone (41). Numerous mechanisms probably converge in the selection of relapse ALL clones at relapse, particularly considering the complexity of multiagent chemotherapy protocols used in the treatment of this disease. However, our analysis of protein–protein interaction networks of relapse-associated mutant factors supports that, at least in part, relapse-associated mutations may converge in common nodes related to escape from DNA damage response (TP53) and glucocorticoid resistance (CREBBP and NR3C1). The positive selection of resistance-driving genetic alterations at relapse implies that chemotherapy inflicts a strong Darwinian selection for drug resistance and argues against genetic drift of passenger mutations or competition for empty bone marrow niche space after chemotherapy as drivers of clonal evolution during leukemia progression.

RAS-activating mutations are rare in unselected newly diagnosed ALL, yet they were present in over 40% of ALL matched diagnosis-relapsed samples, supporting an association of these genetic alterations with high-risk ALL. However, the pattern of clonal evolution of RAS mutations is highly heterogeneous, with some leukemias showing retention of the diagnostic-associated RAS mutations at relapse and some others showing gain or loss of RAS mutations during disease progression. This phenomenon, first reported in early mutation analyses over 25 y ago (43) and recently confirmed in the context of contemporary therapies (18, 31), supports that RAS mutations are frequently subclonal and that the evolutionary pressure imposed by multiagent chemotherapy can result in positive but also negative selection of RAS mutant clones at relapse. Functional analyses of RAS mutations in mouse primary isogenic leukemia lymphoblasts and in human cell lines supports a role of RAS-MAPK signaling in methotrexate resistance but also, and most unexpectedly, implicates oncogenic RAS in the deregulation of the mitotic machinery and in increased sensitivity to vincristine. The development of leukemia models with subclonal RAS mutations will facilitate the analysis of clonal evolution of RAS mutant populations at different stages of disease progression and in the context of chemotherapy treatment in vivo. In addition, analysis of serial leukemia clinical samples from ALL patients receiving multiagent therapy will facilitate better understanding of the dynamics of RAS mutant clones in the context of clinically relevant drug exposure in vivo. Finally, it is worth noting that although less frequent, activating mutations in other signaling factors (e.g., JAK2 and FLT3) also showed a mixed pattern of clonal selection at relapse, which warrants further studies to evaluate their potential differential response to cytotoxic drugs in ALL.

Materials and Methods

DNAs from leukemic ALL blasts at diagnosis and relapse and matched remission lymphocytes were obtained with informed consent in a multi-institutional setting. Informed consent was obtained at study entry, and samples were collected under the supervision of local Institutional Review Boards for participating institutions and analyzed under the supervision of the Columbia University Medical Center Institutional Review Board. We selected samples for whole-exome and whole-genome sequencing on the basis of the availability of sufficient DNA from diagnosis, remission, and relapse samples. Sample size was determined to have 95% power to detect recurrent mutations present in over 5% of samples and 78% power to detect these as recurrent in at least two samples. Animal procedures were performed in accordance and with approval from the Columbia University Institutional Animal Care and Use Committee.

Genomic Analyses. Whole-exome sequencing was performed using the Agilent SureSelect Human 51 Mb All Exon V4 kit (Agilent Technologies) platform and paired-end sequencing on the Illumina HiSeq2000 System. Somatic sequence variants were identified using the SAVI algorithm (19). Somatic CNVs

were identified from the depth of coverage using EXCAVATOR (44). Whole-genome sequencing libraries were prepared using the Illumina TruSeq Nano DNA Sample Prep Kit, and sequencing was performed on Illumina HiSeq X Ten instrument (Illumina). Paired-end (2 × 150 bp) reads were aligned to the GRCh37 human reference using the Burrows–Wheeler Aligner (BWA aln) (45). Variant callers muTect v1.1.4 (46) and Strelka v1.0.12 (47) (for both SNVs and indels) were used, and the resulting SNV and indels were annotated via snpEff (48). For analysis of RNAseq samples, we identified variants in 18 selected relapse-associated genes using the SAVI algorithm. We identified variants that differed from the reference genome in targeted resequencing data on 614 amplicons from 18 genes generated using the Access Array system from Fluidigm and analyzed them by paired-end sequencing (2 × 150 bp) in a NextSeq500 instrument (Illumina) using the SAVI algorithm.

In Vitro Studies. We determined cell viability by measurement of the metabolic reduction of the tetrazolium salt MTT using the Cell Proliferation Kit I (Roche) following the manufacturer's instructions. We analyzed apoptosis by flow cytometry with APC AnnexinV apoptosis Kit I (BD Biosciences) and 4′,6-Diamidino-2-phenylindole dihydrochloride. We performed cell-cycle analysis by flow cytometry analysis of DNA content using Hoechst 33342 (Sigma Aldrich) staining. All assays were performed in triplicates and reproduced at least twice.

We performed Western blot analysis using antibodies recognizing P-ERK1/2 [P-P44/P42 MAPK (T202/Y204)] (1:1,000; 4377, Cell Signaling Technology), ERK1/2 (1:250; sc-271270, Santa Cruz Biotechnologies), P-PLK1 [P-T210] (1:1,000; Abcam), PLK [F8] (1:50; sc-17783, Santa Cruz Biotechnologies), and GAPDH (1:7,000; 5174, Cell Signaling Technology), following standard procedures.

Statistical Analyses. Analyses of significance were performed using Student's *t* test assuming equal variance and Fisher's exact test. Continuous biological variables were assumed to follow a normal distribution. A two-sided *P* value of <0.05 was considered to indicate statistical significance.

ACKNOWLEDGMENTS. This work was supported by a Leukemia & Lymphoma Quest for Cures award (to A.A.F.); an Innovative Research award (to A.A.F.); a Phillip A. Sharp Innovation in Collaboration award by Stand Up to Cancer (to A.A.F.); the St. Baldrick's Foundation (A.A.F.); the Chemotherapy Foundation (A.A.F.); the Swim Across America Foundation (A.A.F.); NIH Grants R01 CA185486 (to R.R.), U54 CA193313 (to R.R.), and U10 CA98543 (to J.M.G.-F. and M.L.L.); Human Specimen Banking Grant U24 CA114766 (to J.M.G.-F.); Cariparo Foundation and Istituto di Ricerca Pediatrica-Città della Speranza (IRP) Foundation (G.B.); and the Stewart Foundation (R.R.). G.T. is a Howard Hughes Medical Institute International Student Research Fellow. M.S.-M. is a Rally Foundation fellow.

1. Chan KW (2002) Acute lymphoblastic leukemia. *Curr Probl Pediatr Adolesc Health Care* 32(2):40–49.
2. Coebergh JW, et al. (2006) Leukaemia incidence and survival in children and adolescents in Europe during 1978-1997. Report from the Automated Childhood Cancer Information System project. *Eur J Cancer* 42(13):2019–2036.
3. Inaba H, Greaves M, Mullighan CG (2013) Acute lymphoblastic leukaemia. *Lancet* 381(9881):1943–1955.
4. Siegel R, Naishadham D, Jemal A (2013) Cancer statistics, 2013. *CA Cancer J Clin* 63(1):11–30.
5. Mitchell C, Richards S, Harrison CJ, Eden T (2010) Long-term follow-up of the United Kingdom medical research council protocols for childhood acute lymphoblastic leukaemia, 1980-2001. *Leukemia* 24(2):406–418.
6. Pui CH, Evans WE (2006) Treatment of acute lymphoblastic leukemia. *N Engl J Med* 354(2):166–178.
7. Bhojwani D, Pui CH (2013) Relapsed childhood acute lymphoblastic leukaemia. *Lancet Oncol* 14(6):e205–e217.
8. Guan Y, Gerhard B, Hogge DE (2003) Detection, isolation, and stimulation of quiescent primitive leukemic progenitor cells from patients with acute myeloid leukemia (AML). *Blood* 101(8):3142–3149.
9. Iwamoto S, Mihara K, Downing JR, Pui CH, Campana D (2007) Mesenchymal cells regulate the response of acute lymphoblastic leukemia cells to asparaginase. *J Clin Invest* 117(4):1049–1057.
10. Yang Y, et al. (2013) Wnt pathway contributes to the protection by bone marrow stromal cells of acute lymphoblastic leukemia cells and is a potential therapeutic target. *Cancer Lett* 333(1):9–17.
11. Tzoneva G, et al. (2013) Activating mutations in the NT5C2 nucleotidase gene drive chemotherapy resistance in relapsed ALL. *Nat Med* 19(3):368–371.
12. Meyer JA, et al. (2013) Relapse-specific mutations in NT5C2 in childhood acute lymphoblastic leukemia. *Nat Genet* 45(3):290–294.
13. Göker E, et al. (1995) Amplification of the dihydrofolate reductase gene is a mechanism of acquired resistance to methotrexate in patients with acute lymphoblastic leukemia and is correlated with p53 gene mutations. *Blood* 86(2):677–684.
14. Hsiao MH, Yu AL, Yeargin J, Ku D, Haas M (1994) Nonhereditary p53 mutations in T-cell acute lymphoblastic leukemia are associated with the relapse phase. *Blood* 83(10):2922–2930.
15. Kuster L, et al. (2011) ETV6/RUNX1-positive relapses evolve from an ancestral clone and frequently acquire deletions of genes implicated in glucocorticoid signaling. *Blood* 117(9):2658–2667.
16. Mullighan CG, et al. (2011) CREBBP mutations in relapsed acute lymphoblastic leukaemia. *Nature* 471(7337):235–239.
17. Mar BG, et al. (2014) Mutations in epigenetic regulators including SETD2 are gained during relapse in paediatric acute lymphoblastic leukaemia. *Nat Commun* 5:3469.
18. Ma X, et al. (2015) Rise and fall of subclones from diagnosis to relapse in pediatric B-acute lymphoblastic leukaemia. *Nat Commun* 6:6604.
19. Trifonov V, Pasqualucci L, Tiacci E, Falini B, Rabadan R (2013) SAVI: A statistical algorithm for variant frequency identification. *BMC Syst Biol* 7(Suppl 2):S2.
20. Mullighan CG (2012) Molecular genetics of B-precursor acute lymphoblastic leukemia. *J Clin Invest* 122(10):3407–3415.
21. Weng AP, et al. (2004) Activating mutations of NOTCH1 in human T cell acute lymphoblastic leukemia. *Science* 306(5694):269–271.
22. Thompson BJ, et al. (2007) The SCFFBW7 ubiquitin ligase complex as a tumor suppressor in T cell leukemia. *J Exp Med* 204(8):1825–1835.
23. Van Vlierberghe P, et al. (2010) PHF6 mutations in T-cell acute lymphoblastic leukemia. *Nat Genet* 42(4):338–342.
24. Tosello V, et al. (2009) WT1 mutations in T-ALL. *Blood* 114(5):1038–1045.
25. Della Gatta G, et al. (2012) Reverse engineering of TLX oncogenic transcriptional networks identifies RUNX1 as tumor suppressor in T-ALL. *Nat Med* 18(3):436–440.
26. De Keersmaecker K, et al. (2013) Exome sequencing identifies mutation in CNOT3 and ribosomal genes RPL5 and RPL10 in T-cell acute lymphoblastic leukemia. *Nat Genet* 45(2):186–190.
27. Zhang J, et al. (2012) The genetic basis of early T-cell precursor acute lymphoblastic leukaemia. *Nature* 481(7380):157–163.
28. Mathur D, Somashekar S, Navarrete C, Rodriguez MM (2014) Twin infant with lymphatic dysplasia diagnosed with Noonan syndrome by molecular genetic testing. *Fetal Pediatr Pathol* 33(4):253–257.
29. Tartaglia M, et al. (2006) Diversity and functional consequences of germline and somatic PTPN11 mutations in human disease. *Am J Hum Genet* 78(2):279–290.
30. Irving J, et al. (2014) Ras pathway mutations are prevalent in relapsed childhood acute lymphoblastic leukemia and confer sensitivity to MEK inhibition. *Blood* 124(23):3420–3430.
31. Malinowska-Ozdowy K, et al. (2015) KRAS and CREBBP mutations: A relapse-linked malicious liaison in childhood high hyperdiploid acute lymphoblastic leukemia. *Leukemia* 29(8):1656–1667.
32. Pear WS, et al. (1996) Exclusive development of T cell neoplasms in mice transplanted with bone marrow expressing activated Notch alleles. *J Exp Med* 183(5):2283–2291.
33. Caunt CJ, Sale MJ, Smith PD, Cook SJ (2015) MEK1 and MEK2 inhibitors and cancer therapy: The long and winding road. *Nat Rev Cancer* 15(10):577–592.
34. Jackman M, Lindon C, Nigg EA, Pines J (2003) Active cyclin B1-Cdk1 first appears on centrosomes in prophase. *Nat Cell Biol* 5(2):143–148.
35. Macůrek L, et al. (2008) Polo-like kinase-1 is activated by aurora A to promote checkpoint recovery. *Nature* 455(7209):119–123.
36. van Vugt MA, Brás A, Medema RH (2004) Polo-like kinase-1 controls recovery from a G2 DNA damage-induced arrest in mammalian cells. *Mol Cell* 15(5):799–811.
37. Holleman A, et al. (2004) Gene-expression patterns in drug-resistant acute lymphoblastic leukemia cells and response to treatment. *N Engl J Med* 351(6):533–542.
38. Papaemmanuil E, et al. (2014) RAG-mediated recombination is the predominant driver of oncogenic rearrangement in ETV6-RUNX1 acute lymphoblastic leukemia. *Nat Genet* 46(2):116–125.
39. Nabel CS, Manning SA, Kohli RM (2012) The curious chemical biology of cytosine: Deamination, methylation, and oxidation as modulators of genomic potential. *ACS Chem Biol* 7(1):20–30.
40. Ding L, et al. (2008) Somatic mutations affect key pathways in lung adenocarcinoma. *Nature* 455(7216):1069–1075.
41. Ding L, et al. (2012) Clonal evolution in relapsed acute myeloid leukaemia revealed by whole-genome sequencing. *Nature* 481(7382):506–510.
42. Mullighan CG, et al. (2008) Genomic analysis of the clonal origins of relapsed acute lymphoblastic leukemia. *Science* 322(5906):1377–1380.
43. Neri A, Knowles DM, Greco A, McCormick F, Dalla-Favera R (1988) Analysis of RAS oncogene mutations in human lymphoid malignancies. *Proc Natl Acad Sci USA* 85(23):9268–9272.
44. Magi A, et al. (2013) EXCAVATOR: Detecting copy number variants from whole-exome sequencing data. *Genome Biol* 14(10):R120.
45. Li H, Durbin R (2009) Fast and accurate short read alignment with Burrows-Wheeler transform. *Bioinformatics* 25(14):1754–1760.
46. Cibulskis K, et al. (2013) Sensitive detection of somatic point mutations in impure and heterogeneous cancer samples. *Nat Biotechnol* 31(3):213–219.
47. Saunders CT, et al. (2012) Strelka: Accurate somatic small-variant calling from sequenced tumor-normal sample pairs. *Bioinformatics* 28(14):1811–1817.
48. Cingolani P, et al. (2012) A program for annotating and predicting the effects of single nucleotide polymorphisms, SnpEff: SNPs in the genome of *Drosophila melanogaster* strain w1118; iso-2; iso-3. *Fly (Austin)* 6(2):80–92.